

Article

Not peer-reviewed version

Cyanide Molecular Laser-Induced Breakdown Spectroscopy with Current Databases

[Christian Parigger](#) *

Posted Date: 27 February 2023

doi: 10.20944/preprints202302.0430.v1

Keywords: diatomic molecules; cyanide; laser-plasma; data analysis; laser induced breakdown spectroscopy; combustion; time-resolved spectroscopy; spectra fitting program; astrophysics



Preprints.org is a free multidiscipline platform providing preprint service that is dedicated to making early versions of research outputs permanently available and citable. Preprints posted at Preprints.org appear in Web of Science, Crossref, Google Scholar, Scilit, Europe PMC.

Copyright: This is an open access article distributed under the Creative Commons Attribution License which permits unrestricted use, distribution, and reproduction in any medium, provided the original work is properly cited.

Article

Cyanide Molecular Laser-Induced Breakdown Spectroscopy with Current Databases

Christian G. Parigger * 

Physics and Astronomy Department, University of Tennessee, University of Tennessee Space Institute, Center for Laser Applications, 411 B.H. Goethert Parkway, Tullahoma, TN 37388-9700, USA; cparigge@tennessee.edu

* Correspondence: cparigge@tennessee.edu; Tel.: +1 (931) 841 5690

Abstract: This work discusses diatomic molecular spectroscopy of laser-induced plasma and analysis of data records, specifically signatures of cyanide, CN. Line strength data from various databases are compared for simulation of the CN, $B^2\Sigma^+ \rightarrow X^2\Sigma^+$, $\Delta v = 0$ sequence. Of interest are recent predictions using an astrophysical database, i.e., ExoMol, a laser-induced fluorescence database, i.e., LIFBASE, and a program for simulating rotational, vibrational and electronic spectra, i.e., PGOPHER. Cyanide spectra that are predicted from these databases are compared with line strength data that are in use by the author for the last three decades in the analysis of laser-plasma emission spectra. Comparisons with experimental laser-plasma records are communicated as well, and for spectral resolutions of 33 and 110 picometer. The accuracy of the CN line strength data is better than one picometer. Laboratory experiments utilize 308-nm, 35-picosecond bursts within an overall 1-nanosecond pulse-width, and 1064-nm, 6-ns pulse-width radiation. Experimental results are compared with predictions. Differences of the databases are elaborated for equilibrium of rotational and vibrational modes and at an internal, molecular temperature of the order of 8,000 Kelvin. Applications of accurate CN data include for example combustion diagnosis, chemistry, and supersonic and hypersonic expansion diagnosis. The cyanide molecule is also of interest in the study of astrophysical phenomena.

Keywords: diatomic molecules; cyanide; laser-plasma; data analysis; laser induced breakdown spectroscopy; combustion; time-resolved spectroscopy; spectra fitting program; astrophysics

1. Introduction

The diatomic molecule cyanide, CN, occurs in various forms in nature. Toxicity of cyanide motivates health studies, in particular those of hydrogen cyanide gas that kills by inhalation. Cyanide radical measurements characterize interstellar clouds including temperature inferences of the cosmic microwave background radiation [1,2]. The primary interest in this work are the CN violet $B^2\Sigma^+ - X^2\Sigma^+$ band systems. Extensive experimental and theoretical details convey the complexity of the CN radical [3,4]. Particularly the CN red systems are mentioned in a study of laboratory spectroscopy of astrophysically interesting molecules [5].

Spectroscopy [6–10] of laser-induced air plasma reveals “fingerprints” of CN early (within the first microsecond) in the plasma decay [11]. Recent developments of laser-induced breakdown spectroscopy indicate interests in diagnosis of molecular species. This work investigates existing databases for diatomic molecules, in particular the ones for CN, for analysis of measured emission spectra. Laser-induced breakdown with 6-ns, 1064-nm radiation and associated diagnosis [12] discusses determination of CN distribution and shock-wave phenomena in hypersonic and supersonic expansion.

For cyanide spectroscopy, one can employ the ExoMol database [13], the LIFBASE laser-induced fluorescence database [14], and the PGOPHER program for simulating rotational, vibrational and electronic spectra [15]. There are of course other databases that can be accessed [16] for diatomic molecules, including HITEMP that for example shows hydroxyl, OH, data [17]. The ExoMol, LIFBASE, PGOPHER predictions of the CN violet $\Delta v = 0$ sequence are compared with experimental data. The

laser-plasma recombination spectra that are utilized in the comparisons were captured following optical breakdown with picosecond laser pulses in a 1:1 molar CO₂:N₂ atmospheric gas mixture and in standard ambient temperature and pressure laboratory conditions. Astrophysical ExoMol databases are expected to work well for optical spectroscopy of laser-plasma. The measurement of molecular spectra may be accomplished with nanosecond laser-induced optical breakdown - molecular spectra are readily observed with femtosecond or picosecond laser-plasma excitation - after some time delay (of the order of larger than 100 ns for occurrence of CN in CO₂:N₂ gas mixtures) from optical breakdown when using nanosecond laser pulses. In addition, analysis is discussed with previously established line-strength data that are freely available along with MATLAB [18] scripts for a subset of transitions associated with the CN violet and red band systems [19,20].

2. Materials and Methods

Computation of optical molecular spectra relies on sets of wavelength positions and line strengths for molecular band systems with in principle theoretically resolved vibrational and rotational transitions. Experimental spectral resolutions discussed in this work are 0.033 nm to 0.11 nm. Consequently, there are a multitude of lines for each wavelength-bin of a digital array detector that captures time-resolved data following individual laser-plasma events. For example, there are well over 2,000 lines in the CN violet Δv = 0 spectral region of 370 nm to 390 nm, and most lines are bunched together including overlapped vibrational band heads. The measurements utilize a typical laser-induced optical breakdown experimental arrangement [21], namely, (i) laser device, (ii) focusing lens, (iii) cell that contains the atmospheric mixture, (iv) spectrometer, (v) linear diode detector and optical multichannel analyzer, (vi) electronic timing, and (vii) monitor devices and equipment for subsidiary measurements capturing time-resolved CN B-X data

2.1. Traditional simulation of diatomic molecular spectra

The traditional approach for the generation of simulated spectra is based on molecular constants. The energy levels can be evaluated by employing a Dunham expansion [22],

E(v, J) = ∑_{k,l} Y_{k,l} (v + 1/2)^k [J(J + 1)]^l. (1)

The constant coefficients Y_{k,l} are called Dunham parameters, with the indices k and l corresponding to vibrational and rotational contributions, respectively. The k = 0 and l = 0 parameter Y_{0,0} represents the minimum electronic energy, T_e. Table 1 lists the molecular constants in units of cm⁻¹ for the A–X and B–X transitions for ¹²C¹⁴N [23].

Table 1. Spectroscopic constants for the A–X and B–X transitions of ¹²C¹⁴N.

Y _{k,l}	Constant	X ² Σ ⁺ (cm ⁻¹)	A ² Π (cm ⁻¹)	B ² Σ ⁺ (cm ⁻¹)
Y _{0,0}	T _e	0.	9,245.28	25,752.0
Y _{1,0}	ω _e	2,068.59	1,812.5	2,163.9
Y _{2,0}	−ω _e x _e	13.087	12.60	20.2
Y _{3,0}	ω _e y _e	−0.00909	−0.0118	−
Y _{0,1}	B _e	1.8997	1.7151	1.973
Y _{1,1}	−α _e	0.01736	0.01708	0.023
Y _{2,1}	γ _e	−3.10 × 10 ^{−5}	−3.6 × 10 ^{−5}	−
Y _{0,2}	−D _e	6.40 × 10 ^{−6}	5.93 × 10 ^{−6}	[6.6 × 10 ^{−6}]
Y _{1,2}	−β _e	1.2 × 10 ^{−9}	42 × 10 ^{−9}	−

The application of traditional molecular constants (see Table 1) is expected to reveal line-position and intensity inconsistencies. For example, air emission spectra predictions with the non-equilibrium air radiation (NEQAIR) code [24,25] reveal slightly different line positions leading to difficulties in air-plasma analysis of superposition spectra composed of several species. The laser plasma that is

generated in dry air shows a variety of species [26–28], consequently, accurate predictions of individual components are desirable. Recently, commercial SPECAIR software is available that focuses on calculating emission or absorption spectra of air plasma radiation [29]. Conversely, one can utilize published molecular line positions and strengths for individual species for the spectra simulation of the CN diatomic molecule, as further elaborated in Sections 2.2, 2.3 and 2.4.

2.2. Line positions and strengths of diatomic spectra

In this work, the computation of diatomic molecular spectra utilizes line strength data. The Boltzmann equilibrium spectral program (BESP) and the Nelder-Mead temperature (NMT) program allow one to respectively compute an emission spectrum and fit theoretical to experimental spectra. The construction of the communicated molecular CN line strengths “CNv-lsf” [20] first, makes use of Wigner-Witmer eigenfunctions and a diatomic line position fitting program, second, computes Frank-Condon factors and r-centroids, and third, combines these factors with the rotational factors that usually decouple from the overall molecular line-strength due to the symmetry of diatomic molecules. In turn, the ExoMol states and transition files for CN [4,30,31] and the PGOPHER data file [32] are examined in order to generate line strength data that can be used with BESP and NMT. The LIFBASE program is utilized for visual comparisons of CN B-X simulated and recorded data.

The ExoMol and the PGOPHER data show Einstein A-coefficients that are converted to line strengths [33–35], S , for electric dipole transitions, using

$$A_{ul} = \frac{16\pi^3}{3g_u h \epsilon_0 \lambda^3} (e a_0)^2 S_{ul}, \quad g_u = 2(2J_u + 1). \quad (2)$$

Here, A_{ul} denotes the Einstein A-coefficient for a transition from an upper, u , to a lower, l , state, and h and ϵ_0 are Planck’s constant and vacuum permittivity, respectively. The elementary charge is e , the Bohr radius is a_0 , and the transition strength is S_{ul} . The line strength, S , that is used in the MATLAB scripts is expressed in traditional spectroscopy units ($\text{stC}^2 \text{cm}^2$). The wavelength of the transition is λ , g_u is the upper state degeneracy and J_u the total angular momentum of the upper state.

2.3. Wigner-Witmer diatomic eigenfunction

The Hund’s case (a) basis functions (explicitly, see Eq. (6) below) are derived from the Wigner and Witmer [36,37] diatomic eigenfunction,

$$\langle \rho, \zeta, \chi, \mathbf{r}_2, \dots, \mathbf{r}_N, r, \theta, \phi | n v J M \rangle = \sum_{\Omega=-J}^J \langle \rho, \zeta, \mathbf{r}'_2, \dots, \mathbf{r}'_N, r | n v \rangle D_{M\Omega}^{J*}(\phi, \theta, \chi). \quad (3)$$

The coordinates include the distance, ρ , of one electron (the electron arbitrarily labeled 1 but it could be any one of the electrons) from the internuclear vector, $\mathbf{r}(r, \theta, \phi)$, the distance, ζ , of that electron above or below the plane perpendicular to \mathbf{r} and passing through the center of mass of the two nuclei (the coordinate origin), the angle, χ , for rotation of that electron about the internuclear vector \mathbf{r} , and the remaining electronic coordinates $\mathbf{r}_2, \dots, \mathbf{r}_N$ in the fixed and $\mathbf{r}'_2, \dots, \mathbf{r}'_N$ in the rotating coordinate system. The vibrational quantum number v has been extracted from the quantum number collection n that represents all required quantum numbers except J , M , Ω , and v . The Wigner-Witmer diatomic eigenfunction is well-suited for the description of the diatomic molecule. The exact separation of the Euler angles represents a clear advantage over the Born-Oppenheimer approximation for the diatomic molecule in which the angle of electronic rotation, χ , is unnecessarily separated from the angles describing nuclear rotation, θ and ϕ . Equation (3) can be derived by writing the general equation for coordinate (passive) rotations α , β , and γ of the eigenfunction, replacing two generic coordinate vectors with the diatomic vectors $\mathbf{r}(r, \theta, \phi)$ and $\mathbf{r}'(\rho, \zeta, \chi)$, and equating the angles of coordinate rotation to the angles of physical rotation ϕ , θ , and ϕ . The general equation for coordinate rotation holds in isotropic

space, and therefore the quantum numbers J , M , and Ω , in the Wigner-Witmer eigenfunction include all electronic and nuclear spins.

The rotation matrix element $D_{M\Omega}^J(\phi, \theta, \chi)$ and its complex conjugate $D_{M\Omega}^{J*}(\phi, \theta, \chi)$ do not fully possess the mathematical properties of quantum mechanical angular momentum. It is well known that a sum of Wigner D -functions is required to build an angular momentum state. The equation

$$J'_{\pm} D_{M\Omega}^{J*}(\phi, \theta, \chi) = \sqrt{J(J+1) - \Omega(\Omega \mp 1)} D_{M, \Omega \mp 1}^{J*}(\phi, \theta, \chi) \quad (4)$$

is a mathematical result readily obtained from Eq. (3) and

$$J'_{\pm} |J\Omega\rangle = \sqrt{J(J+1) - \Omega(\Omega \pm 1)} |J, \Omega \pm 1\rangle, \quad (5)$$

in which the prime on the operator J'_{\pm} indicates that it is written in the rotated coordinate system where the appropriate magnetic quantum number Ω .

The Hund's case (a) basis function based upon the Wigner-Witmer diatomic eigenfunction, with the spin ket $|S\Sigma\rangle$, equals

$$\begin{aligned} |a\rangle &= \langle \rho, \zeta, \chi, \mathbf{r}'_2, \dots, \mathbf{r}'_N, r, \theta, \phi | n\nu J M \Omega L \Lambda S \Sigma \rangle \\ &= \sqrt{\frac{2J+1}{8\pi^2}} \langle \rho, \zeta, \mathbf{r}'_2, \dots, \mathbf{r}'_N, r | n\nu \rangle |S\Sigma\rangle D_{M\Omega}^{J*}(\phi, \theta, \chi). \end{aligned} \quad (6)$$

As noted above, a sum of $|a\rangle$ basis functions is required to build an eigenstate of angular momentum.

The prediction of diatomic spectra and establishment of the CNv-lsf database involves (a) determination of accurate wavenumbers for the transition and rotational line strengths, viz. Hönl-London values (see details below in Section 2.4), (b) vibrational transition strengths, viz. Frank-Condon factors, from eigenfunctions for the diatomic potential, (c) expansion of the electronic transition moments employing r-centroids. The product of these three factors yields the line strength, or alternatively, the Einstein A-coefficient using Eq. (2).

2.4. Diatomic line position fitting algorithm

A traditional task of a diatomic spectroscopist is the computation of a set of molecular parameters from experimentally measured vacuum wavenumbers $\tilde{\nu}_{\text{exp}}$ that are associated with J' and J , and in turn, infer from that set of molecular parameters the $\tilde{\nu}_{\text{exp}}$ with a standard deviation comparable to the estimated experimental error. In practice, an experimental line list frequently shows gaps, viz. spectral lines are missing. Following a successful fitting process, one can use the molecular parameters to predict all lines.

Trial values of upper and lower state molecular parameters, typically taken from previous works by others for the band system in question, are used to compute upper H' and lower H Hamiltonian matrices in the case (a) basis given by Eq. (6) for specific values of J' and J . The upper and lower Hamiltonians are numerically diagonalized,

$$T' = \tilde{U}' H' U' \quad (7a)$$

$$T = \tilde{U} H U \quad (7b)$$

giving the upper T' and lower T term values. The vacuum wavenumbers $\tilde{\nu}$, labeled using i and j for the dimensions (levels) of the upper and lower Hamiltonians,

$$\tilde{\nu}_{ij} = T'_i - T_j, \quad (8)$$

are determined, and the rotational strength,

$$S_{ij}(J', J) = (2J + 1) \left| \sum_n \sum_m \tilde{U}'_{in} \langle J\Omega; q, \Omega' - \Omega | J'\Omega' \rangle U_{mj} \delta(\Sigma'_n \Sigma_m) \right|^2, \quad (9)$$

is evaluated. The degree of the tensor operator, q , responsible for the transitions amounts to $q = 1$ for electric dipole transitions. For a non-zero rotational factors, $S(J', J)$, the vacuum wavenumber $\tilde{\nu}_{ij}$ is added to a table of computed line positions to be compared with the experimental list $\tilde{\nu}_{\text{exp}}$ versus J' and J . The Clebsch-Gordan coefficient, $\langle J\Omega; q, \Omega' - \Omega | J'\Omega' \rangle$, is the same one appearing in the pure case (a) - case (a) formulae for $S(J', J)$. For specific values of J' and J , one constructs tables for $\tilde{\nu}_{\text{exp}}$ and computed $\tilde{\nu}_{ij}$. The errors $\Delta\tilde{\nu}_{ij}$,

$$\Delta\tilde{\nu}_{ij} = \tilde{\nu}_{ij} - \tilde{\nu}_{\text{exp}}, \quad (10)$$

are computed where each $\tilde{\nu}_{ij}$ is the one that most closely equals one of the $\tilde{\nu}_{\text{exp}}$. Once values of $\tilde{\nu}_{ij}$ and $\tilde{\nu}_{\text{exp}}$ are matched, each is marked unavailable until a new list of $\tilde{\nu}_{ij}$ is computed. The indicated computations are performed for all values of J' and J in the experimental line list, and corrections to the trial values of the molecular parameters are subsequently determined from the resulting $\Delta\tilde{\nu}_{ij}$. The entire process is iterated until the parameter corrections become negligibly small. As this fitting process successfully concludes, one obtains a set of molecular parameters that predict the measured line positions $\tilde{\nu}_{\text{exp}}$ with a standard deviations that essentially equal the experimental estimates for the accuracy of the $\tilde{\nu}_{\text{exp}}$. Of course, once sets of transition lines and strengths along with appropriate designations are determined for a particular diatomic molecule, one can employ these sets (that so-to-speak resemble a digital “fingerprint” of the diatomic molecule) in the analysis of recorded spectra.

2.5. Measured air wavelength vs. vacuum wavenumbers

The PGOPHER program allows versatile fitting of experimental data records by introducing a so-called overlay data set as function of wavenumbers. Experimental data are converted to vacuum wavenumbers using the variation of the refractive index, n , of air with wavelength [38],

$$10^6(n - 1) = a_0 + \frac{a_1}{\lambda_N^2} + \frac{a_2}{\lambda_N^4}, \quad (11)$$

where λ_N is the wavelength in normal air at 15 °C and 101,325 Pa (760 mm Hg), expressed in terms of micrometer (range 0.2218–0.9000 μm). Table 2 lists constants for Eq. (11).

Table 2. Constants for variation of refractive index, n , see Equation 11.

Parameter	Value
a_0	272.643
a_1	1.2288 (μm^2)
a_2	0.03555 (μm^4)

For NMT computations however recorded, digital intensity values versus calibrated wavelength are utilized. The variation of the refractive index, r_i , of air at 15 °C, 101,325 Pa, and 0% humidity, with wavenumber [39],

$$10^8(r_i - 1) = \frac{k_1}{(k_0 - \sigma^2)} + \frac{k_3}{(k_2 - \sigma^2)}, \quad (12)$$

where σ is the wavenumber in units of μm^{-1} , allows one to compute air wavelengths from the vacuum wavenumbers. Table 3 lists constants in Eq. (12).

Table 3. Constants for variation of refractive index, see Equation 12.

Parameter	Value (μm^{-2})
k_0 (k0)	238.0185
k_1 (k1)	5,792,105
k_2 (k2)	57.362
k_3 (k3)	167,917

3. Results

This section elaborates analysis of recorded CN spectra of the $\text{B } ^2\Sigma^+ \rightarrow \text{X } ^2\Sigma^+, \Delta v = 0$ sequence. The PGOPHER-program analysis is discussed first. The full CN B-X and A-X transition data are available for the construction of simulated spectra. Figure 1 displays measured and fitted CN violet spectra. The fitted spectrum also shows the baseline correction and difference between experimental and simulated spectra.

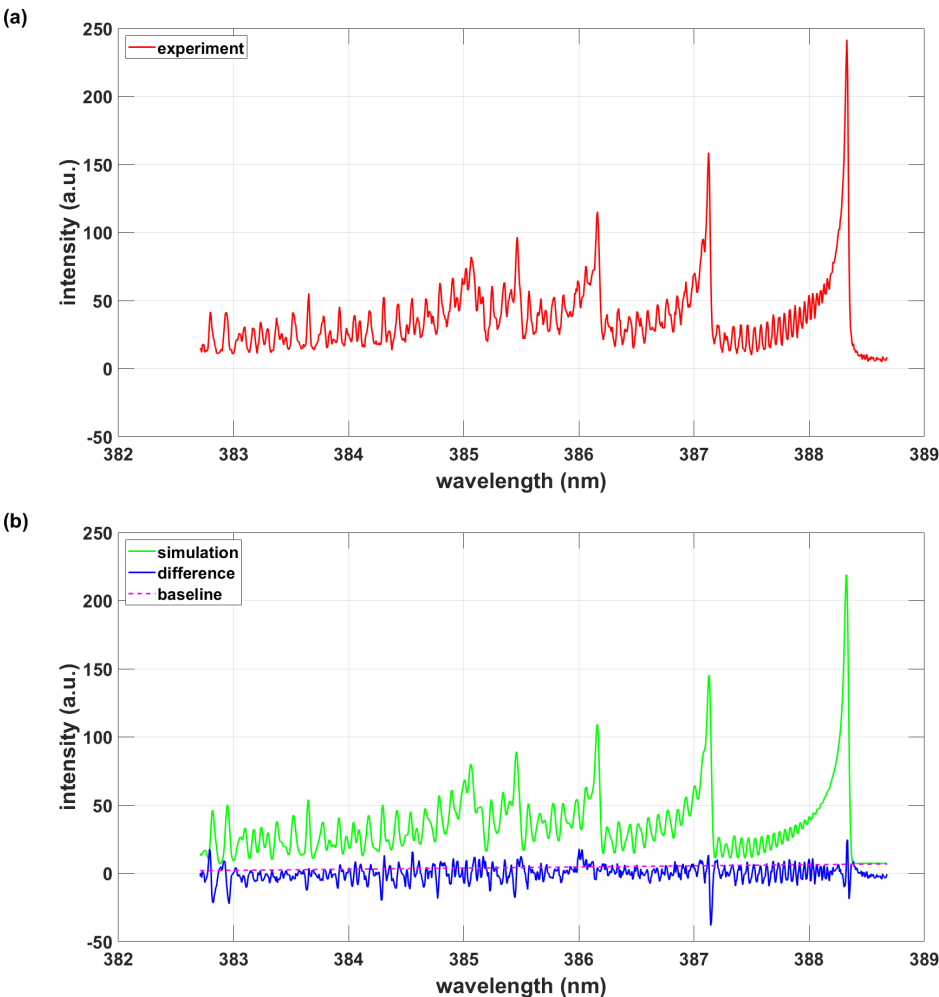


Figure 1. (a) Experimental spectrum. (b) Simulation with PGOPHER, $T = 8103 \text{ K}$, $\Delta\lambda = 0.033 \text{ nm}$.

The spectra were captured using an intensified 1024-diode array detector and a laboratory-type Czerny-Turner (Jobin Yvon model HR-640, Fr) spectrometer. The spectral resolutions of the experimental arrangement amount to 0.11 nm ($\simeq 7 \text{ cm}^{-1}$) and 0.033 nm ($\simeq 2 \text{ cm}^{-1}$) for the employed 1200 and 3600 groves/mm gratings, respectively. The time-resolved measurement gate-delays were 400 nanosecond (ns), with gate-open times of 500 ns and 600 ns for the higher and lower resolution

data, respectively. An average of 40 spectra were collected, consequently, the inferred temperature is an average of the line-of-sight data during the gate-open duration.

The synthetic spectrum is fitted using the PGOPHER program and an overlay of the experimental record of recorded optical multichannel analyzer (OMA) counts versus vacuum wavenumbers that are computed from the recorded air wavelengths. Table 4 lists results for parameters that were selected for fitting. Normalized intensity units were used, i.e., the partition function is implemented. Following a separate fit for determination of the wavenumber offset of -0.31 cm^{-1} (-0.005 nm - the Doppler width at $\simeq 8,000\text{ K}$ for CN equals $\simeq 0.005\text{ nm}$), the selected parameters included Gaussian width, temperature, scaling, and T_{vib} that assesses deviation from thermodynamic equilibrium. The T_{vib} results confirms Boltzmann distribution equilibrium within the standard deviation.

Table 4. PGOPHER fitting parameters for the 0.033-nm data and results.

Parameter	Value	Standard Deviation
Temperature (K)	8,103	187
Gaussian width (cm^{-1})	2.2	0.03
Scale (a.u.)	43,960	790
T_{vib} (K)	8,108	146

In addition, CN B-X line positions and Einstein A-coefficients (that are converted to line strengths) are collected in a data file that is compatible with the mentioned NMT-spectral fitting program. Figure 2 illustrates spectra determined from temperature and Gaussian linewidth fitting. The results are consistent with those obtained from the versatile PGOPHER program. The inclusion of CN A-X data in the analysis would change the inferred temperature by $\simeq 0.1\%$.

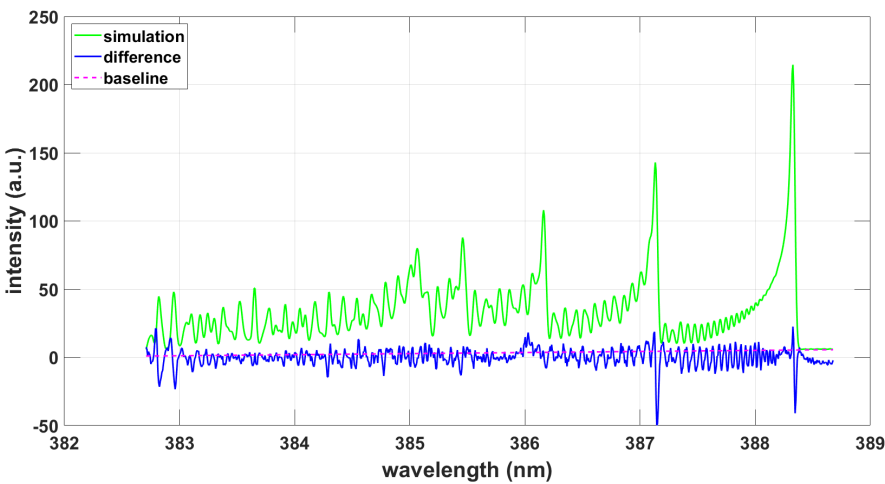


Figure 2. Simulation using PGOPHER data and the NMT program, $T = 8240\text{ K}$, $\Delta\lambda = 0.034\text{ nm}$.

Similarly, the recommended ExoMol databases for states and transitions were utilized to generate a subset of lines and strength for analysis with the NMT program and for the 0.033-nm resolution data. The results displayed in Figure 3 indicate a Gaussian full-width-at-half-maximum (FWHM) of 0.038 nm, indicative of line-position differences in the ExoMol data. However, the inferred temperature appears consistent with the results illustrated in Figures 1 and 2.

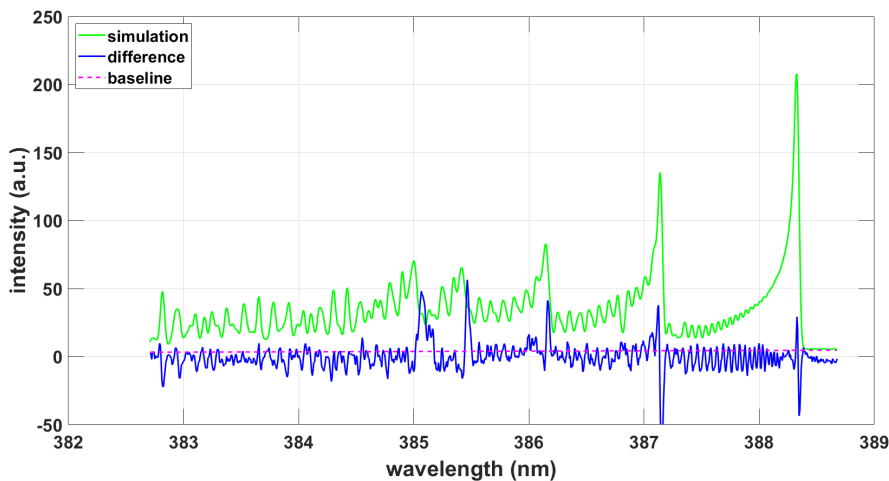


Figure 3. Simulation using ExoMol data and the NMT program, $T = 8150\text{ K}$, $\Delta\lambda = 0.038\text{ nm}$.

Analysis of the measured data with the CNv-lsf data reveals a temperature of $T = 8140\text{ K}$, and a fitted FWHM of 0.038 nm . Figure 4 shows the fitting results.

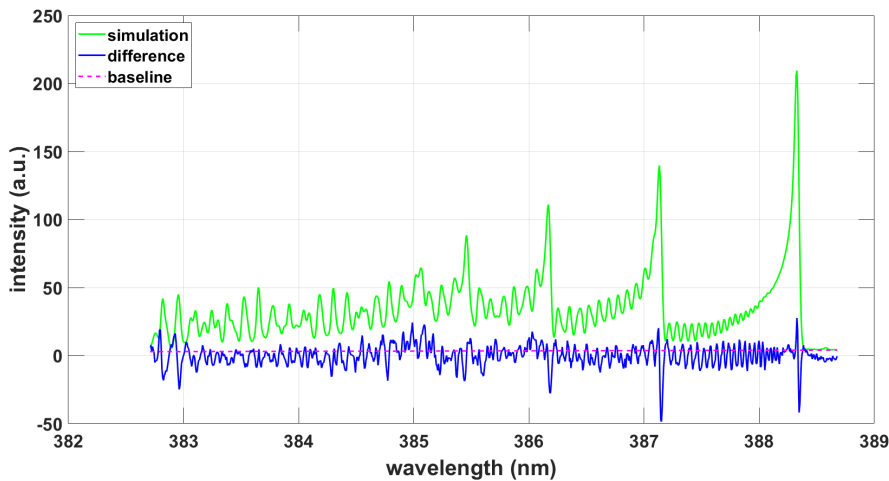


Figure 4. Simulation using CNv-lsf data and the NMT program, $T = 8140\text{ K}$, $\Delta\lambda = 0.036\text{ nm}$.

The simulated spectra in Figures 1, 2, 3, and 4, display superposition spectra from quite a few individual rotational-vibrational transitions of the CN B-X $\Delta v = 0$ sequence. Actually, small contributions from the CN A-X transition are also included in the PGOPHER and ExoMol databases. Tables 5 and 6 summarize the number of lines in the data files.

Table 5. Number of transitions of the simulated spectra in the measured experimental ranges for the 0.033-nm ($25,725\text{ cm}^{-1}$ to $26,125\text{ cm}^{-1}$) and 0.11-nm ($25,600\text{ cm}^{-1}$ to $27,600\text{ cm}^{-1}$) data.

Database	0.033-nm range CN B-X	0.033-nm range CN B-X and A-X	0.11-nm range CN B-X	0.11-nm range CN B-X and A-X
PGOPHER	3,598	5,631	7,115	14,349
ExoMol	4,302	17,181	10,499	78,079
CNv-lsf	2,461	2,461	3,313	3,313

Table 6. Number of transitions of the simulated spectra in the measured experimental ranges for the 0.033-nm and 0.11-nm (see Tab. 5) with Einstein A-coefficients larger than 10^3 s^{-1} .

Database	0.033-nm range CN B-X	0.033-nm range CN B-X and A-X	0.11-nm range CN B-X	0.11-nm range CN B-X and A-X
PGOPHER	3,205	4,532	6,187	9,958
ExoMol	3,625	8,270	8,259	28,274
CNv-lsf	2,461	2,461	3,313	3,313

Comparisons of CN B-X line position accuracies in the PGOPHER and ExoMol databases with those of the CNv-lsf database are further elaborated for the range of the 0.033-nm resolution experiments ($25,725 \text{ cm}^{-1}$ to $26,125 \text{ cm}^{-1}$) and for Einstein A-coefficients larger than 10^3 s^{-1} (see first column in Table 6). Table 7 displays agreements of lines within the indicated wavenumber range and otherwise the same angular momentum values for upper and lower levels of the transitions.

Table 7. Subset CN B-X lines of the PGOPHER and ExoMol data that agree within $\Delta\tilde{\nu}$ of 2,461 CN B-X transitions in the CNv-lsf data for the 0.033-nm range ($25,725 \text{ cm}^{-1}$ to $26,125 \text{ cm}^{-1}$).

Database	$\Delta\tilde{\nu} < 0.05 \text{ cm}^{-1}$	$\Delta\tilde{\nu} < 0.2 \text{ cm}^{-1}$	$\Delta\tilde{\nu} < 1.0 \text{ cm}^{-1}$	$\Delta\tilde{\nu} < 2.0 \text{ cm}^{-1}$
PGOPHER	1,200	1,422	1,823	2,012
ExoMol	158	463	1,266	1,935

Various aspects of the accuracy of the CNv-lsf database have been extensively tested [19] including analysis of laser-induced fluorescence and nominal 300 K temperature Fourier transform spectra. The differences in predictions for line positions appears larger for levels with higher angular momenta, J' and J . The accuracy of line positions in the CNv-lsf database is better than 0.05 cm^{-1} . Table 7 reveals that PGOPHER line positions compare favorably with those in the CNv-lsf database. The ExoMol database appears acceptable within $\simeq 2$ wavenumbers that corresponds to a spectral resolution of $\simeq 0.033 \text{ nm}$. However, high-temperature ($\simeq 8,000 \text{ K}$) inferences from CN B-X spectra at a 0.033-nm experimental spectral resolution appear only minimally affected (see Figures 2 and 3).

In addition, the LIFBASE program is used for simulation of the measured spectrum. A Voigt profile of width 0.033 nm with a 30% Lorentzian contribution is selected. Figure 5 illustrates the results. Noteworthy is that the PGOPHER program is capable of fitting Voigt profiles as well. However, Gaussian profiles are usually selected in the NMT program for modeling of the spectrometer & detector transfer function.

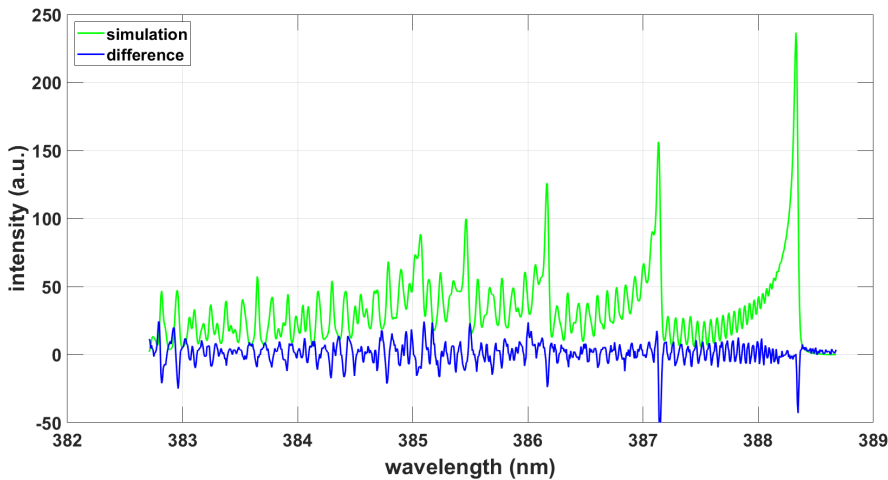


Figure 5. Simulation using LIFBASE with fixed $T = 8103 \text{ K}$, $\Delta\lambda = 0.033 \text{ nm}$, Voigt profile with 30% Lorentzian contribution.

One of the primary interests is the use of updated ExoMol sets of line strength data that appear to be in use for extragalactic studies [31]. Availability of an extensive line list obviously would alleviate

computation of specific transitions that are investigated in laser-plasma laboratory experiments, including CN B-X violet and CN A-X red systems. The ExoMol database shows 2,285,103 transitions up to $60,000\text{ cm}^{-1}$ between the three lowest electronic states, $X^2\Sigma^+$, $A^2\Pi$, and $B^2\Sigma^+$. The PGOPHER dataset for CN A-X and B-X includes 191,109 transitions.

The CNv-lsf and CNr-lsf data contain 7,960 and 40,728 transitions, respectively. The differences in number of transitions are in part due to the number of rotational states (up to $\simeq 120$ in ExoMol), the cutoffs for Einstein A-coefficients and associated line strengths (see Eq. (2)), or the establishment of sets of computed molecular parameters that fit data from high-resolution, Fourier-transform spectroscopy. As communicated in Section 2.4, the line positions are determined from high-resolution data with a standard deviation comparable to the estimated experimental errors. The obtained, simulated line strengths are typically better than 0.05 cm^{-1} .

The lower resolution, 0.11-nm data are analyzed using a similar approach as that for the 0.033-nm data. Following a separate fit for determination of the wavenumber offset of 0.13 cm^{-1} (0.002 nm), the selected parameters included Gaussian width, temperature, and scaling. Figure 6 illustrates the results obtained by employing the PGOPHER fitting program and the available, full CN B-X and CN A-X data set [32]. The effect of the CN A-X transition lines is minimal for temperature inference, viz. 0.1% for the higher spectral resolution data (see Fig. 2).

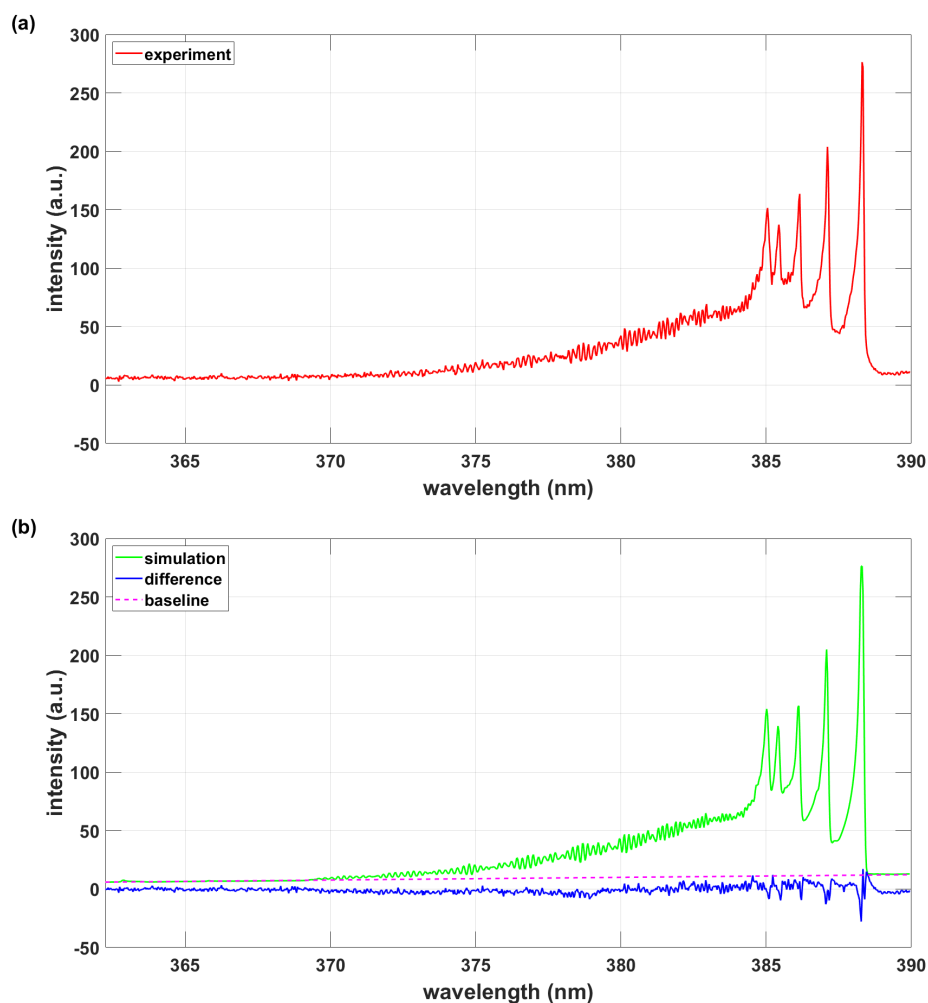


Figure 6. (a) Experimental spectrum. (b) Simulation with PGOPHER, $T = 8340\text{ K}$, $\Delta\lambda = 0.11\text{ nm}$.

Table 8 summarizes the results of PGOPHER fitting including the standard deviations.

Table 8. PGOPHER fitting parameters for the 0.11-nm data and results.

Parameter	Value	Standard Deviation
Temperature (K)	8,340	43
Gaussian width (cm ⁻¹)	7.1	0.07
Scale (a.u.)	107,300	850

Figure 7 displays the results of the NMT-program using PGOPHER data. As before, the NMT-program resorts to fitting of relative intensities. In turn, the scales that are indicated in Tabs. 4 and 8 can serve as a calibration of the detector counts in the laboratory recorded CN spectra.

The fitting of the experimental data using the PGOPHER-extracted wavenumbers, upper term values and Einstein A-coefficients (that are converted to line strengths) with the NMT program shows similar results as obtained for exclusive PGOPHER fitting.

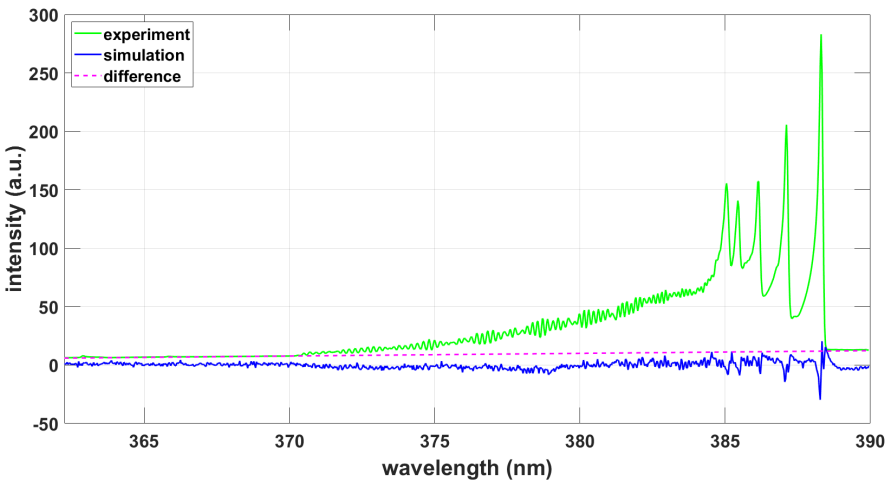


Figure 7. Simulation using PGOPHER data and the NMT program, T = 8380 K, $\Delta\lambda = 0.11$ nm.

The fitting ExoMol data using the NMT program yields a temperature of T = 9090 K for a spectral resolution of $\Delta\lambda = 0.11$ nm. Figure 8 illustrates the simulated spectrum, difference and baseline. A temperature of T = 8940 K is obtained when using CNv-lsf in the NMT program. Figure 9 shows the results.

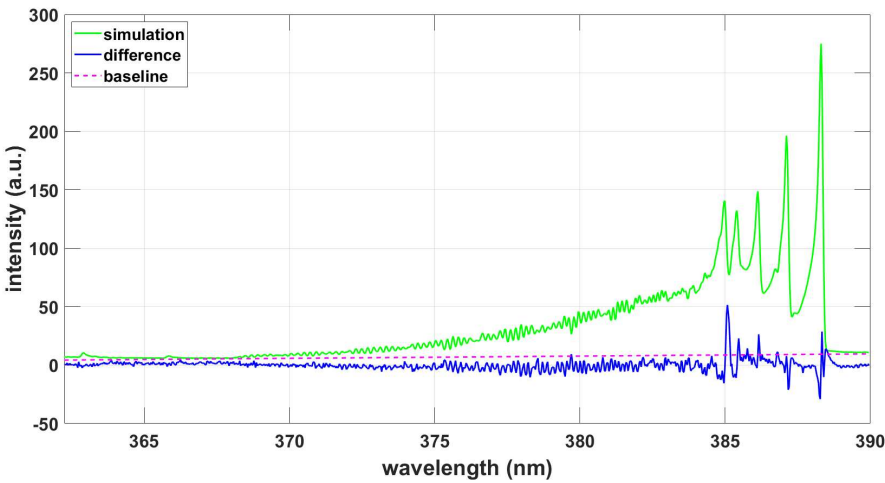


Figure 8. Simulation using ExoMol data and the NMT program, T = 9090 K, $\Delta\lambda = 0.11$ nm.

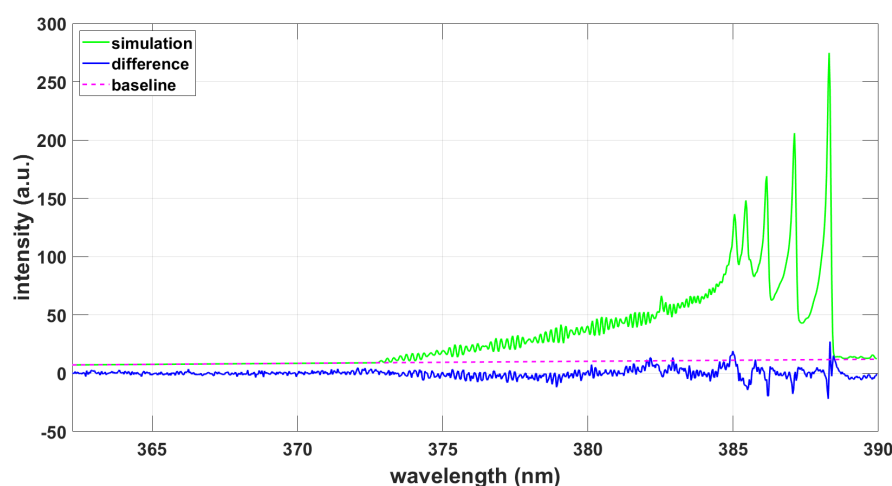


Figure 9. Simulation using CNv-lsf data and the NMT program, $T = 8940$ K, $\Delta\lambda = 0.11$ nm.

4. Discussion

The CN violet $B^2\Sigma^+ - X^2\Sigma^+$, $\Delta v = 0$ sequence reveals a multitude of vibrational and rotational transitions that are usually not individually resolved in the study of laser-induced plasma emissions in the spectral range of 383 nm to 389 nm. Analysis of the 0.033-nm spectral resolution experimental emission spectrum with the PGOPHER program and use of full CN B-X data file yields CN excitation temperature of $\simeq 8,100$ K and a standard deviation of $\simeq 200$ K.

Similar results are obtained when using the CN B-X data in conjunction with a Nelder-Mead spectral fitting program. The most recent ExoMol CN data also predict a temperature within the standard deviation of the PGOPHER prediction, but there appear to be discrepancies in the ExoMol predictions near the 2-2, 3-3, and 4-4 band heads, or in the range of 385 nm to 386 nm. Analogous results are noted when using the CNv-lsf line strengths with however slightly better agreement of experimental and simulated spectra than those for ExoMol. Comparative spectra obtained from the LIFBASE program are as well largely in agreement with the measured data.

The lower, 0.11-nm resolution data in the range of 362 nm to 390 nm appear to be well predicted by the PGOPHER data. About 6% higher temperatures are predicted with the ExoMol and the CNv-lsf data. The CN violet spectra have been extensively tested in a variety of experimental studies of laser plasma.

For comprehensive comparisons of experimental and simulated spectra however the higher the spectral resolution the better. The expansive PGOPHER and ExoMol line lists allow one to predict simulated spectra consistent with laboratory laser-plasma experiments.

Funding: This research received no specific external funding.

Acknowledgments: The author (CGP) acknowledges the support in part by the Center for Laser Applications at the University of Tennessee Space Institute. Furthermore, deep appreciation goes to departed J.O. Hornkohl and C.M. Western for their meticulous work in quantum mechanics of the diatomic molecule and contributions toward simulating rotational, vibrational and electronic spectra, and their contributions, respectively, to the development of BESP, NMT, and PGOPHER programs.

Institutional Review Board Statement: Not applicable.

Informed Consent Statement: Not applicable.

Data Availability Statement: Not applicable.

Conflicts of Interest: The author declares no conflict of interest. The funders had no role in the design of the study; in the collection, analyses, or interpretation of data; in the writing of the manuscript, or in the decision to publish the results.

Abbreviations

The following abbreviations are used in this manuscript:

BESP	Boltzmann equilibrium spectral program
CNv-lsf	Cyanide violet system line strength data
ExoMol	Molecular line lists for exoplanet and other hot atmospheres
FWHM	Full-Width at half maximum
HITEMP	High temperature molecular spectroscopic database
LIFBASE	Program for simulating selected diatomic molecules
LSF	Line strength file
NEQAIR	Non-Equilibrium air radiation
NIST	National Institute of Standards and Technology
NMT	Nelder-Mead temperature
OMA	Optical multichannel analyzer
PGOPHER	Program for simulating rotational, vibrational and electronic spectra
SATP	Standard ambient temperature and pressure
SPECAIR	Program for calculating emission or absorption spectra of air plasma radiation

References

- Roth, K.C.; Meyer, D.M.; Hawkins, I. Interstellar cyanogen and the temperature of the cosmic microwave background radiation. *Astrophys. J.* **1993**, *413*, L67–L71.
- Leach S. CN spectroscopy and cosmic background radiation measurements. *Can. J. Chem* **2004**, *82*, 730–739.
- Ram R.S.; Davis S.P.; Wallace L.; Englman R.; Appadoo D.R.T.; Bernath P.F. Fourier transform emission spectroscopy of the $B^2\Sigma^+ - X^2\Sigma^+$ system of CN. *J. Mol. Spectrosc.* **2006**, *37*, 225–231.
- Brooke J.S.A.; Ram R.S.; Western C.M.; Li G.; Schwenke D.W.; Bernath P.F. Einstein A Coefficients and Oscillator Strengths for the $A^2\Pi - X^2\Sigma^+$ (Red) and $B^2\Sigma^+ - X^2\Sigma^+$ (Violet) Systems and Rovibrational Transitions in the $X^2\Sigma^+$ State of CN. *Astrophys. J., Suppl. Ser.* **2014**, *210*, 1–15.
- Davis, S.P. Laboratory spectroscopy of astrophysically interesting molecules. *Publ. Astron. Soc. Pac.* **1987**, *99*, 1105–1114.
- Kunze, H.-J. *Introduction to Plasma Spectroscopy*; Springer: Berlin/Heidelberg, Germany, 2009.
- Fujimoto, T. *Plasma Spectroscopy*; Clarendon Press; Oxford, UK, 2004.
- Ochkin, V.N. *Spectroscopy of Low Temperature Plasma*; Wiley-VCH: Weinheim, Germany, 2009.
- Demtröder, W. *Laser Spectroscopy 1: Basic Principles*, 5th ed.; Springer: Heidelberg, Germany, 2014.
- Demtröder, W. *Laser Spectroscopy 2: Experimental Techniques*, 5th ed.; Springer: Heidelberg, Germany, 2015.
- Miziolek, A.W., Palleschi, V., Schechter, I. (Eds.) *Laser Induced Breakdown Spectroscopy (LIBS): Fundamentals and Applications*; Cambridge Univ. Press: New York, NY, USA, 2006.
- Singh, J.P.; Thakur, S.N. (Eds.) *Laser-Induced Breakdown Spectroscopy*, 2nd ed.; Elsevier: Amsterdam, The Netherlands, 2020.
- Tennyson, J.; Yurchenko, S.N.; Al-Refaie, A.F.; Clark, V.H.J.; Chubb, K.L.; Conway, E.K.; Dewan, A.; Gorman, M.N.; Hill, C.; Lynas-Gray, A.E.; Mellor, T.; McKemmish, L.K.; Owens, A.; Polyansky, O.L.; Semenov, M.; Somogyi, W.; Tinetti, G.; Upadhyay, A.; Waldmann, I.; Wang, Y.; Wright, S.; Yurchenko, O.P. The 2020 release of the ExoMol database: Molecular line lists for exoplanet and other hot atmospheres. *J. Quant. Spectrosc. Radiat. Transf.* **2020**, *255*, 107228.
- Luque, J.; Crosley, D.R. LIFBASE: Database and Spectral Simulation for Diatomic Molecules. **2021**. Available online <https://www.sri.com/platform/lifbase-spectroscopy-tool> (accessed on 25 November 2019).
- Western, C.M. PGOPHER, A Program for Simulating Rotational, Vibrational and Electronic Spectra. *J. Quant. Spectrosc. Radiat. Transf.* **2017**, *186*, 221–242.
- McKemmish, L.K. Molecular diatomic spectroscopy data. *WIREs Comput. Mol. Sci.* **2021**, *11*, e1520.
- Rothman, L.S.; Gordon, I.E.; Barber, R.J.; Dothe, H.; Gamache, R.R.; Goldman, A.; Perevalov, V.I.; Tashkun, S.A.; Tennyson, J. HITEMP, the high-temperature molecular spectroscopic database. *J. Quant. Spectrosc. Radiat. Transf.* **2010**, *111*, 2139–2150.
- MATLAB Release R2022a Update 5, The MathWorks, Inc.: Natick, Massachusetts, US, 2022.
- Parigger, C.G.; Hornkohl, J.O. *Quantum Mechanics of the Diatomic Molecule with Applications*; IOP Publishing: Bristol, UK, 2020.
- Parigger, C.G. Diatomic line strengths for fitting selected molecular transitions of ALO, C₂, CN, OH, N₂⁺, NO, and TiO, spectra. *Foundations* **2023**, *3*, 1–15.

21. Hornkohl, J.O.; Parigger, C.G.; Lewis, J.W.L. Temperature Measurement from CN spectra in a laser-induced plasma. *J. Quant. Spectrosc. Radiat. Transf.* **1991**, *46*, 405–411.
22. Dunham, J.L. The Energy Levels of a Rotating Vibrator. *Phys. Rev.* **1932**, *41*, 721–731.
23. National Institute of Standards and Technology (NIST) Chemistry WebBook, SRD 69, for the Cyano radical, constants of diatomic molecules. **2021**. Available online <https://webbook.nist.gov> (accessed on 20 February 2023).
24. Whiting E.E. Space Administration, Reacting Flow Environments Branch, Ames Research Center, CA, US. Personal communication, 1995.
25. Whiting, E.E.; Park, C.; Liu, Y.; Arnold, J.; Paterson, J. *Technical Report NASA RP-1389*; NASA Ames Research Center: Moffet Field, CA, US, 1996.
26. Boulous, P.M.I.; Pfender, E. *Thermal Plasmas - Fundamentals and Applications*; Plenum Press, New York, NY, US, 1994.
27. McBride, B.; Gordan, S. *Interim Revision NASA Report RP-1311, Part I*; NASA Lewis Research Center: Cleveland, OH, US, 1994.
28. McBride, B.; Gordan, S. *Interim Revision NASA Report RP-1311, Part II*; NASA Lewis Research Center: Cleveland, OH, US, 1996.
29. Laux, C.O. *Radiation and Nonequilibrium Collisional-Radiative Models, von Karman Institute Lecture Series 2002-07, Physico-Chemical Modeling of High Enthalpy and Plasma Flows*, Fletcher D.; Charbonnier, J.-M.; Sarma, G.S.R.; Magin, T. (Eds.): Rhode-Saint-Genèse, Belgium, 2002.
30. Syme, A.-M.; McKemmish, L.K. Experimental energy levels of $^{12}\text{C}^{14}\text{N}$ through MARVEL analysis. *Mon. Notices Royal Astron. Soc.* **2020**, *499*, 25–39.
31. Syme, A.M.; McKemmish, L.K. Full spectroscopic model and trihybrid experimental-perturbative-variational line list for CN. *Mon. Notices Royal Astron. Soc.* **2021**, *505*, 4383–4395.
32. Western, C.M. University of Bristol, Bristol, UK. Personal communication, 2019.
33. Condon E.U.; Shortley G.H. *The Theory of Atomic Spectra*; Cambridge Univ Press: Cambridge, UK, 1964.
34. Hilborn R.C. Einstein coefficients, cross sections, f values, dipole moments, and all that. *Am. J. Phys.* **1982**; *50*, 982–986.
35. Thorne A.P. *Spectrophysics*, 2nd ed.; Chapman and Hall: New York, NY, US, 1988.
36. Wigner E.; Witmer E.E. Über die Struktur der zweiatomigen Molekelspektren nach der Quantenmechanik. *Z. Phys.* **1928**, *51*, 859–886.
37. Wigner E.; Witmer E.E. On the structure of the spectra of two-atomic molecules according to quantum mechanics. In Hetttema H. (Ed) *Quantum Chemistry: Classic Scientific Papers*. World Scientific: Singapore, SG, 2000; 287–311.
38. Barrell, H.; Sears, J.E. The Refraction and Dispersion of Air for the Visible Spectrum. *Philos. Trans. Roy. Soc. London* **1939**, Vol. 238, No. 786, 1–64.
39. Ciddor, P.E. Refractive index of air: new equations for the visible and near infrared. *Appl. Opt.* **1996**, *35*, 1567–1573.

Disclaimer/Publisher's Note: The statements, opinions and data contained in all publications are solely those of the individual author(s) and contributor(s) and not of MDPI and/or the editor(s). MDPI and/or the editor(s) disclaim responsibility for any injury to people or property resulting from any ideas, methods, instructions or products referred to in the content.